http://dx.doi.org/10.5012/bkcs.2012.33.11.3761

# $Ag_2Se$-Graphene/$TiO_2$ Nanocomposites, Sonochemical Synthesis and Enhanced Photocatalytic Properties Under Visible Light

**Ze-Da Meng, Lei Zhu, Trisha Ghosh, Chong-Yeon Park, Kefayat Ullah, Vikram Nikam, and Won-Chun Oh†,***

*Department of Advanced Materials Science & Engineering, Hanseo University, Chungnam 356-706, Korea*
**E-mail: wc_oh@hanseo.ac.kr*
*Received June 26, 2012, Accepted August 24, 2012*

$Ag_2Se$-Graphene/$TiO_2$ composite was synthesized by a facile sonochemical method. The as-prepared products were characterized by X-ray diffraction (XRD), Scanning electron microscopy (SEM) with energy dispersive X-ray (EDX) analysis, transmission electron microscopy (TEM) and UV-vis diffuse reflectance spectrophotometer. During the reaction, both of the reduction of graphene oxide and loading of $Ag_2Se$ and $TiO_2$ particles were achieved. The as-prepared $Ag_2Se$-Graphene/$TiO_2$ composites possessed great adsorptivity of dyes, extended light absorption range, and efficient charge separation properties simultaneously. Hence, in the photodegradation of rhodamine B (Rh.B), a significant enhancement in the reaction rate was observed with $Ag_2Se$-Graphene/$TiO_2$ composites, compared to the pure $TiO_2$. The high activity can be attributed to the synergetic effects of high charge mobility, and red shift in absorption edge of $Ag_2Se$-Graphene/$TiO_2$ composites.

**Key Words :** $Ag_2Se$, Graphene, UV-vis absorption spectra, Visible light, Rhodamine B

## Introduction

Graphene is a new star on applications of condensed-matter physics, electronics, and material science after carbon nanotube and $C_{60}$.[1] Because graphene is a single-atom thick sheet arranged by $sp^2$-bonded carbon atoms in a hexagonal lattice, which shows outstanding mechanical, thermal, optical, and electrical properties. Therefore, graphene-based composite materials have attracted much attention as recent studies have shown their usefulness in electronics, photocatalysis and photovoltaic devices.[2-4]

It was reported that nanocarbon materials as CNT and $C_{60}$ have some benecial effects on the photocatalytic activity of homogeneous and heterogeneous semiconductors by effective electron transfer and interaction effects.[5-7] Among the various semiconductors, titanium dioxide ($TiO_2$) is known to be a good catalyst for the degradation of environmental contaminants due to its high photocatalytic activity.[8,9] These $TiO_2$-nanocarbon composite exhibited higher photocatalytic performance than that of bare $TiO_2$. However, some problems still hinder further promotion of efciency of $TiO_2$-nanocarbon composites, such as the weakening of light intensity arriving at surface of catalysts and the lack of reproducibility due to the preparation and treatment variation. [10] In comparison with CNT and $C_{60}$, graphene has perfect $sp^2$-hybridized two-dimensional carbon structure with better conductivity and larger surface area, it seems reasonable to envision that the novel graphene-$TiO_2$ nanocomposite with high interfacial contact and potential could be much more promising to improve the photocatalytic performance of $TiO_2$.[11-14] Furthermore, graphene is easy to produce from inexpensive natural graphite through intermediates product "graphite oxide".[15,16] The presence of oxygen-containing functional groups in graphene oxide (GO) and reduced graphene oxide (RGO) makes them as excellent supporters to anchor $TiO_2$ nanocrystals for the synthesis of graphene-$TiO_2$.[14,17]

Another important feature of the coupled semiconductor system is that the photoresponse of a large band gap semiconductor can be extended into the visible region by coupling it with a short band gap semiconductor.[18-20] Metal selenides have attracted much attention during the past few years due to their special electronic and optical properties and potential applications.[21] Silver selenide exists as a low-temperature phase (β-$Ag_2Se$), and a high-temperature phase (α-$Ag_2Se$) with the phase transition point at 1331 °C.[22] α-$Ag_2Se$ is a well-known superionic conductor that is useful as the solid electrolyte in photochargeable secondary batteries. β-$Ag_2Se$ is a narrow-band-gap semiconductor and has been widely used for a photosensitizer in photo-graphic films or thermalchromic materials. Zhao *et al.*[23] reported fabricated $TiO_2$/$Ag_2Se$ interface composite film by interface reaction of $AgNO_3$ with $NaSeSO_3$ on the activated surface of porous $TiO_2$ film, which has good photovoltaic property and high photocurrent response for visible light. Cao *et al.*[24] reported synthesized Single-crystalline $Ag_2Se$ complex nanostructures *via* a solvothermal route and characterization its photocatalytic activity by photodegradation of rhodamin B (RhB) dye under ultraviolet (UV) light irradiation.

In this work, we present the studies on the preparation of $Ag_2Se$-Graphene/$TiO_2$ composites using a facile sonochemical method and utilization for photodegradation of Rh.B aqueous solution under visible light irradiation. $Ag_2Se$-Graphene/$TiO_2$ composites were characterized by X-ray diffraction (XRD), scanning electron microscopy (SEM) with an energy dispersive X-ray (EDX) analysis, UV-vis diffuse reflectance spectra (DRS). The reasons for improving the photocatalytic activity of $Ag_2Se$-Graphene/$TiO_2$ composites were also dis-

cussed.

## Experimental

**Materials and Reagents.** The titanium (IV) *n*-butoxide (TNB, $C_{16}H_{36}O_4Ti$) as a titanium source for the preparation of $TiO_2$ and graphene/$TiO_2$ composites was purchased from Kanto Chemical Company (Tokyo, Japan). Silver nitrate ($AgNO_3$), Selenium (Se) metal powder and ammonium hydroxide ($NH_4OH$, 28%) were purchased from DaeJung Chemicals & Metal Co., Ltd, Korea. Anhydrous purified sodium sulfite ($Na_2SO_3$, 95%) was purchased from Duksan Pharmaceutical Co., Ltd, Korea. Rh.B ($C_{28}H_{31}ClN_2O_3$, 99.99 + %) was used as model pollutant which purchased from Samchun Pure Chemical Co., Ltd, Korea, respectively. All chemicals used without further purification and all experiments were carried out using distilled water.

**Preparation of $Ag_2Se$-GR/$TiO_2$ Nanocomposite Photocatalyst.** $Ag_2Se$-graphene/$TiO_2$ composites marked as $Ag_2Se$-GR/$TiO_2$ was synthesized by an ultrasonic assisted hydrothermal method[25] with minor modification. GO was synthesized according to the modified Hummers-Offeman method from purified natural graphite in our previous works.[26] A typical experiment for the synthesis of $Ag_2Se$-GR/$TiO_2$ nanocomposite is as follows: Firstly, $Na_2SO_3$ (5 g) and Selenium metal powder (0.5 g) were dissolved in 30 mL distilled water and refluxed for 1 h to form $Na_2SeSO_3$ solution. And 20 mg GO and 22 mg $AgNO_3$ were dispersed into a solution with the molar ratios of ethanol:$H_2O$:TNB = 35:15:4, and nally the suspension was sonicated at room temperature for 1 h using a Controllable Serial-Ultrasonic apparatus (Ultrasonic Processor, VCX 750, Korea). Then, the $Na_2SeSO_3$ solution and 6 mL $NH_4OH$ (28 wt %, pH = 12) were added to above system, and the mixture was stirred rapidly at 100 °C for 8 h. The reaction mixture was allowed to cool to room temperature and the precipitate was filtered, washed with distilled water five times, and dried in a vacuum oven at 80 °C for 12 h before heat treatment at 500 °C for 3 h. Meanwhile, for comparison, another photocatalysts, marked as pure $TiO_2$ and GR-$TiO_2$ were prepared using similar procedure.

**Characterization of Photocatalysts.** The crystallographic structures of the composite photocatalysts were observed by using XRD (Shimatz XD-D1, Japan) at room temperature with Cu Kα radiation (λ = 0.154056 nm) and a graphite monochromator, operated at 40 kV and 30 mA. The BET surface areas of the photocatalysts were determined by measuring nitrogen adsorption at 77 K using a BET analyzer (Monosorb, USA). The morphologies of the photocatalysts were analyzed by SEM (JSM-5200 JOEL, Japan) at 3.0 keV. Transmission electron microscopy (TEM, JEOL, JEM-2010, Japan) with an accelerating voltage of 200 kV was used to examine the size and distribution of the photocatalysts. EDX spectra were also used for elemental analysis of the samples. Raman spectra were utilized to detect possible structural defects in the graphene akes. The measurements were carried out by using a Horiba Jobin Yvon Lab Ram system with a 100 × objective lens and a 532 nm laser excitation. To analyze the light absorption of the photcatalysts, UV-vis absorption spectra was obtained by using a scan UV-vis spectrophotometer (Neosys-2000) equipped with an integrating sphere assembly.

**Measurement of Photocatalytic Activities.** The photocatalytic experiments were performed at ambient temperature to test the ability of the as-prepared composites (pure $TiO_2$, GR-$TiO_2$ and $Ag_2Se$-GR/$TiO_2$) to catalyze the degradation of Rh.B. The visible light sources (λ > 420 nm, LED lamp) were used at a distance of 100 mm from the solution in a darkness box. The initial concentration of Rh.B ($c_0$) was $2.0 \times 10^{-5}$ mol/L. The photocatalyst powder (0.03 g) was dispersed in a 100 mL glass photoreactor containing 100 mL of dye solution. The mixture was sonicated for 10 min and stirred for 30 min in the dark in order to reach adsorption-desorption equilibrium. At the given time intervals a sample of 3.5 mL was taken from the mixture and immediately centrifuged to remove the dispersed photocatalysts. The concentration of the clean transparent solution was analyzed by checking the absorbance at 554 nm for Rh.B with the UV-vis spectrophotometer. The reproducibility was checked by repeating the measurements at least three times and was found to be within the acceptable limit (± 5%).

## Results and Discussion

**Physicochemical Properties.** XRD analysis was used to determine the phase purity and the average crystalline properties of $Ag_2Se$-GR/$TiO_2$ composites are shown in Figure 1. It can be confirmed that the $TiO_2$ in the as-prepared photocatalysts is anatase-phase, while the $Ag_2Se$ appears as the predominant crystalline phase of acanthite. For these three samples, (101), (004), (211), and (204) crystal planes originated from the anatase $TiO_2$ phase while (002), (112), (121), (103), (031), (200), (213), and (134) crystal planes originated from the orthorhombic $Ag_2Se$ phase, which were in accordance with the results reported by Zhan et.al with the lattice parameters were close to a = 4.331 Å, b = 7.061 Å, and c = 7.763 Å (JCPDS card no. 14-0072).[27] No impurity

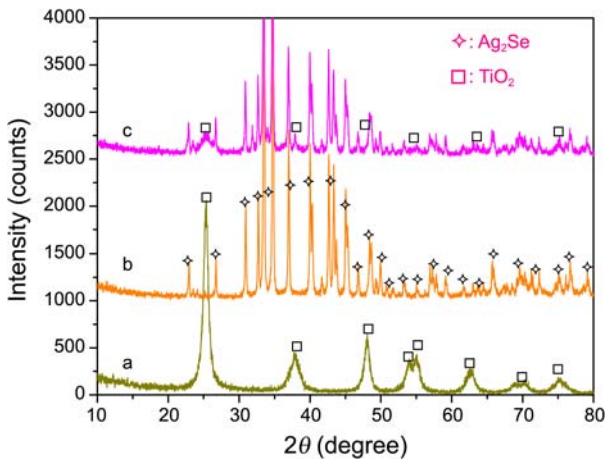


**Figure 1.** XRD patterns of as-prepared samples: (a) $TiO_2$, (b) $Ag_2Se$, (c) $Ag_2Se$-GR/$TiO_2$.

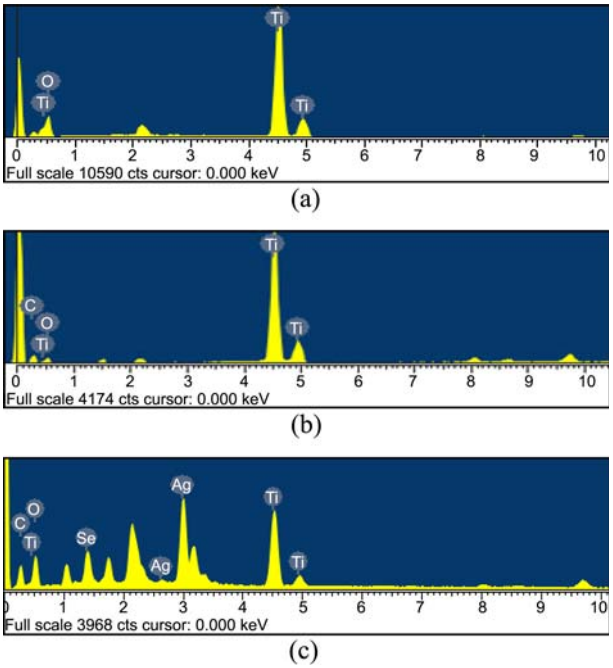


**Figure 2.** EDX elemental microanalysis: (a) $TiO_2$, (b) Graphene-$TiO_2$, (c) $Ag_2Se$-GR/$TiO_2$.

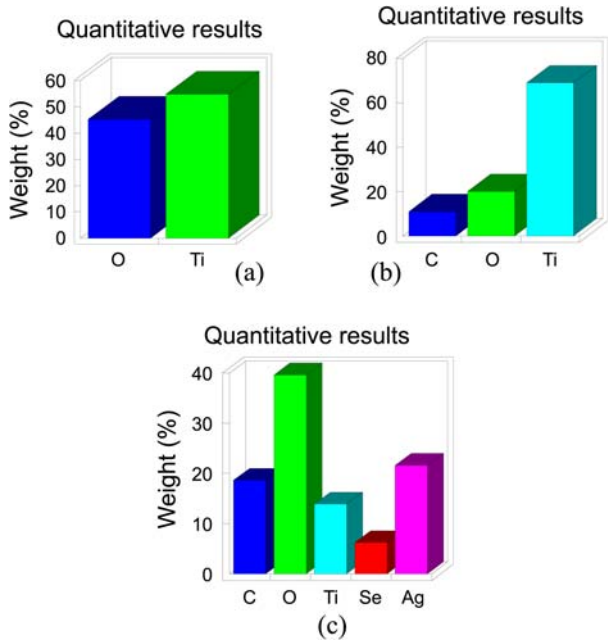


**Figure 3.** Element weight % of as-prepared samples: (a) $TiO_2$, (b) Graphene-$TiO_2$, (c) $Ag_2Se$-GR/$TiO_2$.

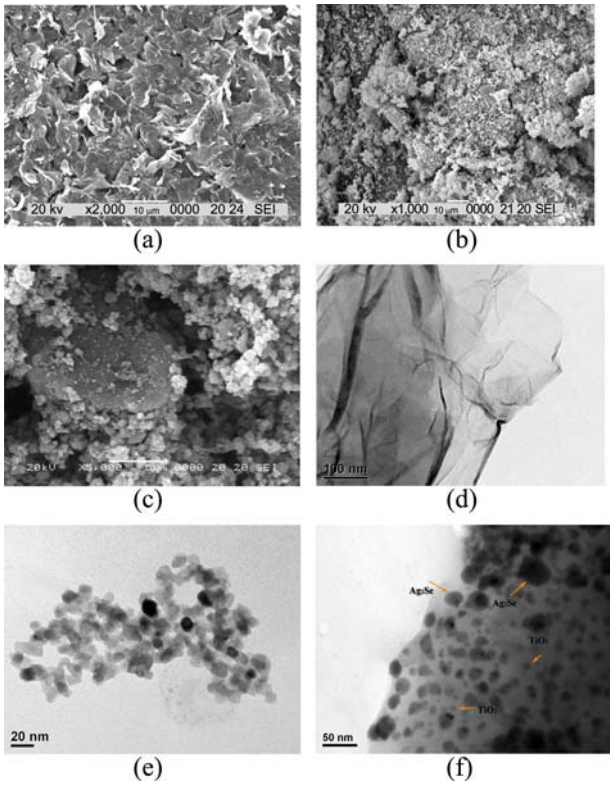


**Figure 4.** SEM (a, b, c) and TEM (d, e, f) micrographs of as-prepared samples: (a, d) Graphene, (b, e) nanoscale $TiO_2$, (c, f) $Ag_2Se$-GR/$TiO_2$.

phase is detected. The broadening of these diffraction peaks indicates that the sample is nanosized. The crystalline size of the sample is estimated to be 15 nm from the Scherrer equation. However, the peak appearing at around 25.88° corresponds to (002) diffraction peak of graphite from the graphene, which is partially overlapped with the (101) crystal plane of anatase $TiO_2$, resulting in the intensity of the (002) diffraction peak to be relatively weak, indicates that the GO has been reduced to graphene, which is in agreement with early reports.[28-30]

The EDX spectra of pure $TiO_2$, GR-$TiO_2$ and $Ag_2Se$-GR/$TiO_2$ composites are shown in Figure 2. These spectra indicate the $TiO_2$ and $Ag_2Se$ with high purity have been successfully synthesized in this study. The C element should mainly originate from graphene sheets. The oxygen and Ti element mainly comes from the $TiO_2$ nanopowder. And the strong Kα and Kβ peaks from Ti element appear at 4.51 and 4.92 keV, while a moderate Kα peak of the element O appears at 0.52 keV.[31] Figure 2 shows the presence of C, O, and Se, as major elements with strong Ag peaks. There were some small impurities, which were attributed to the use of fullerene without purification. In most samples, carbon, silver and selenium were present as major elements with small quantities of oxygen in the composite The elemental microanalyses (wt %) of the samples are listed in Figure 3. According to former studies,[8,9] the higher concentration of dopant in $TiO_2$ matrix can be detrimental in formation of hole/electron recombination centers and an increase of negative charge capabilities.

The typical micro-surface structures and morphologies of the as-prepared composites were characterized by SEM and TEM. The morphology of GO is observed to have aky texture, reecting its layered microstructure, as shown in Figure 4(a). The larger interspaces of the layer and the thinner layer edges of GO can be clearly observed. Simultaneously, it is worth noting that when we used sonochemical method to synthesize control sample and $Ag_2Se$-GR/$TiO_2$

composite, it was clear that the prepared nanoscale $TiO_2$ observed in Figure 4(b) shows a favorable morphology but a little tendency to agglomerate. Compared (b) with (c), very uniform $Ag_2Se$ particles and $TiO_2$ particles can be observed and it was suggested that the graphene introduction contributed the dispersion of $TiO_2$ and $Ag_2Se$ particles on graphene and made these particles appeared uniform. It is reasonable to imagine that such the structure would enable easy charge transfer between the $Ag_2Se$ particles with $TiO_2$ particles and the graphene sheets. And the typical TEM image of as-obtained graphene, $TiO_2$ and $Ag_2Se$-GR/$TiO_2$ composite was displayed in Figure 4(d, e and f). The morphology of GO, consisting of thin stacked akes and having a well-dened few-layer structure at the edge, can be clearly seen in Figure 4(d). Nanoscale $TiO_2$ displayed well-dispersed nanoparticles with an average size of around 10 to 15 nm, can be clearly seen in Figure 4(e). Figure 4(f) reveals a homogeneous dispersion of $TiO_2$ and $Ag_2Se$ nanoparticles attached onto the almost transparent graphene sheets, which may play a support material role in helping $TiO_2$ and $Ag_2Se$ crystals growth. And the average size of well-dispersed $Ag_2Se$ nanoparticles was around 25 to 30 nm. The formation mechanism of $TiO_2$ and $Ag_2Se$ particles itself and the exact role of graphene sheets in this process still await further studies.

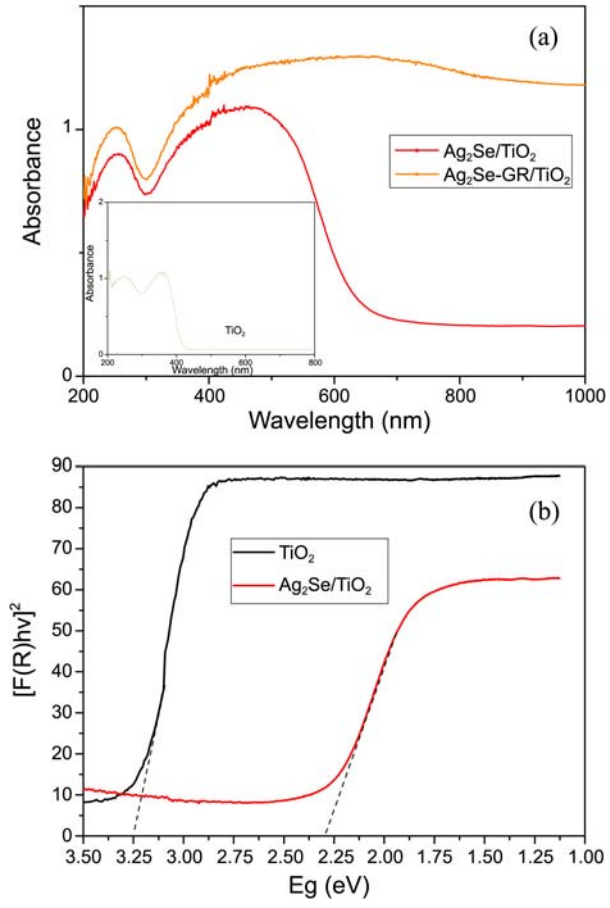


**Figure 5.** (a) UV-vis absorbance spectra of pure $TiO_2$, $Ag_2Se/TiO_2$ and $Ag_2Se$-GR/$TiO_2$; (b) Variation of $(\alpha h\nu)^2$ versus photon energy ($h\nu$) of $TiO_2$ and $Ag_2Se/TiO_2$.

The UV-vis absorption spectra of the different samples are presented in Figure 5(a). As expected, we find that $TiO_2$, $Ag_2Se/TiO_2$ and $Ag_2Se$-GR/$TiO_2$ composites have great absorption in the ultraviolet region. $TiO_2$ shows the characteristic spectrum with its fundamental absorption sharp edge rising at 400 nm (Eg = 3.2 eV). After the introduction of Graphene or $Ag_2Se$ nanoparticles, the absorption edges of $Ag_2Se/TiO_2$ and $Ag_2Se$-GR/$TiO_2$ were shifted toward the visible region, which means that these composites have photocatalytic activity under visible light irradiation. This phenomenon results not only from the excellent conductivity of graphene that can facilitate the separation of photo-generated charges,[32] but also from the introduction of the semiconductor quantum dot $Ag_2Se$ by which the conduction and valence bands of $TiO_2$ are bent downward.[23] The diffuse reflectance spectra of $Ag_2Se/TiO_2$ were transformed by performing the Kubelka-Munk transformation of the measured reflectance according to the following equation;

$$K = (1 - R)^2/2R = F(R) \quad (1)$$

K is reflectance transformed according to Kubelka-Munk, R is reflectance (%), and F(R) is the so-called remission or Kubelka-Munk function. It is well known that the band gap $E_g$, and the absorption coefficient á are related as in following equation;

$$\alpha h\nu = A(h\nu - E_g)^{1/2} \quad (2)$$

where α, $\nu$, $E_g$, and $A$ are the absorption coefficient, light frequency, band gap, and a constant, respectively. If the compound scatters in a perfectly diffuse manner, K becomes equal to $2\alpha$. In this case, we can use the following expression;

$$[F(R)h\nu]^2 = A(h\nu - E_g) \quad (3)$$

The estimated $E_g$ value was 2.31 eV for the $Ag_2Se/TiO_2$ sample. This value is red shifted from the typical $E_g$ of the $TiO_2$ (3.25 eV) in Figure 5(b).

**Degradation Performances.**

**Adsorption Ability:** To evaluate the adsorption ability of the as-prepared composite catalysts, the reactor was placed

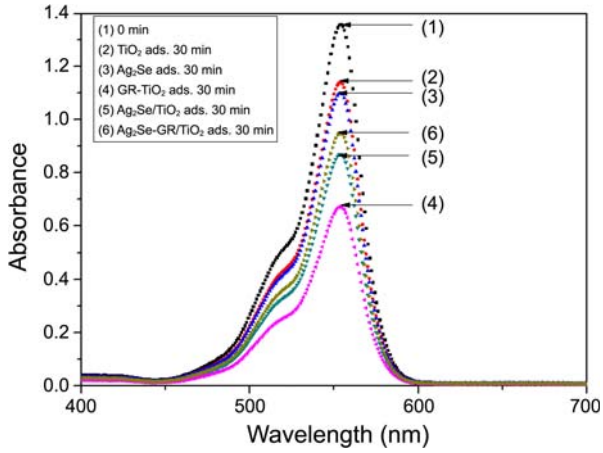


**Figure 6.** UV/Vis spectra of Rh.B concentration against the as-prepared samples after adsorption-desorption equilibrium.

**Table 1.** VL photocatalytic degradation rate ($k_{app}$) constants and BET surface areas of pure $TiO_2$ and $Ag_2Se$-GR/$TiO_2$ catalysts

| Samples | BET ($m^2/g$) | $k_{app}$ ($min^{-1}$) |
|---|---|---|
| pure $TiO_2$ | 11.59 | $5.72 \times 10^{-4}$ |
| $Ag_2Se$ | 17.78 | $1.17 \times 10^{-3}$ |
| GR-$TiO_2$ | 51.95 | $3.94 \times 10^{-3}$ |
| $Ag_2Se/TiO_2$ | 48.32 | $4.25 \times 10^{-3}$ |
| $Ag_2Se$-GR/$TiO_2$ | 45.47 | $6.64 \times 10^{-3}$ |

was placed on the magnetic churn dasher, stirring for 30 min in the darkness box to establish an adsorption-desorption equilibrium. Two steps are involved in the photocatalytic decomposition of dyes: the adsorption of dye molecules and degradation. After adsorption in the dark for 30 min with magnetic stirring, the samples reached adsorption-desorption equilibrium. From the result shown in Figure 6, In the adsorptive step, the level of Rh.B adsorption by $Ag_2Se$-GR/$TiO_2$ was higher than that of the $TiO_2$ powder. This can be attributed to the big surface area of the $Ag_2Se$-GR/$TiO_2$ catalysts shown in Table 1, which correlates to a strong adsorption ability. And sample GR-$TiO_2$ exhibit the best adsorption effect for Rh.B dye solution because the added graphene can enhance the BET surface area which can increase the adsorption effect. After establishing an adsorption-desorption equilibrium, for GR-$TiO_2$ and $Ag_2Se$-GR/$TiO_2$ catalysts the Rh.B dye solution was removed 36% and 30% while Rh.B solution is removed only 16% for pure $TiO_2$. And Figure 7 shows the time series of Rh.B degradation using $Ag_2Se$-GR/$TiO_2$ catalyst under visible light irradiation. The spectra for the Rh.B solution after visible light irradiation show the relative degradation yields at different irradiation times. The dye concentration continuously decreased with an oppositely gentle slope, which was due to visible light irradiation. The concentration of Rh.B was $2.0 \times 10^{-5}$ mol/L, and the absorbance for Rh.B decreased with increasing visible light irradiation time.

Photocatalytic reactions with different photocatalysts can be expressed by the Langmuir-Hinshelwood model.[33] The photocatalytic degradation of Rh.B containing different photo-

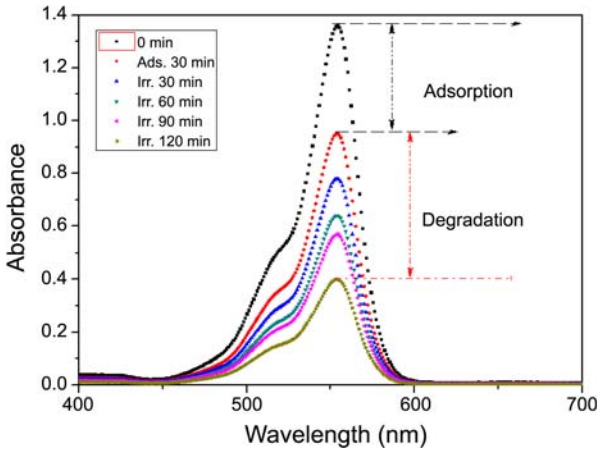


**Figure 7.** UV/Vis spectra of Rh.B concentration against the $Ag_2Se$-GR/$TiO_2$ sample for adsorption and degradation.

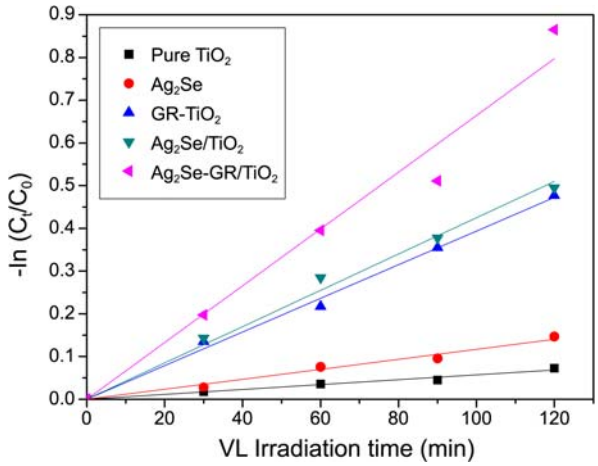


**Figure 8.** Apparent first order kinetics of Rh.B degradation over pure $TiO_2$, $Ag_2Se$, GR-$TiO_2$, $Ag_2Se/TiO_2$ and $Ag_2Se$-GR/$TiO_2$ photocatalysts under visible light irradiation.

catalysts under visible light obeys pseudo-first-order kinetics with respect to the concentration of Rh.B:

$$-dc/dt = k_{app}c \quad (4)$$

Integration of this equation (with the restriction of $c = c_0$ at $t = 0$, with $c_0$ being the initial concentration in the bulk solution after dark adsorption and $t$ the reaction time) will lead to the following expected relation:

$$-\ln(c_t/c_0) = k_{app}t \quad (5)$$

where $c_t$ and $c_0$ are the reactant concentrations at times $t = t$ and $t = 0$, respectively, and $k_{app}$ and $t$ are the apparent reaction rate constant and time, respectively. According to this equation, a plot of $-\ln(c_t/c_0)$ versus $t$ will yield a slope of $k_{app}$. The results are displayed in Figure 8 and also summarized in Table 1. The Rh.B degradation rate constant for $Ag_2Se$-GR/$TiO_2$ composites reaches $6.64 \times 10^{-3}$ $min^{-1}$ under visible light, which are much higher than the corresponding values for pure $TiO_2$, $Ag_2Se$, GR-$TiO_2$ and $Ag_2Se/TiO_2$. The above results suggest that the $Ag_2Se$-GR/$TiO_2$ composites are much more effective photocatalysts than any other composites. The excellent photocatalytic activity could be attributed to the synergetic effects of high charge mobility and the red shift in the absorption edge of the $Ag_2Se$-GR/$TiO_2$ composites.

The excitation scheme and charge transfer process between $Ag_2Se$, $TiO_2$ and graphene nanosheet under visible light irradiation are shown in Figure 9. The UV-vis absorbance spectra (Fig. 5(b)) shown that the band-gap of $Ag_2Se/TiO_2$ nanocomposites is smaller than that of pure $TiO_2$. The narrow band-gap allows $Ag_2Se/TiO_2$ to absorb more photons, and this will enhance the photocatalytic efficiency of $TiO_2$ under visible light irradiation. Because of the inconsistency and overlapping of the conduction band (CB), valence band (VB) and band-gap of the two semiconductors, when $Ag_2Se/TiO_2$ nanocomposites are irradiated under visible light, the photogenerated electrons can be excited from the VB of $Ag_2Se$ and then be transited to the CB of $TiO_2$ photogene-

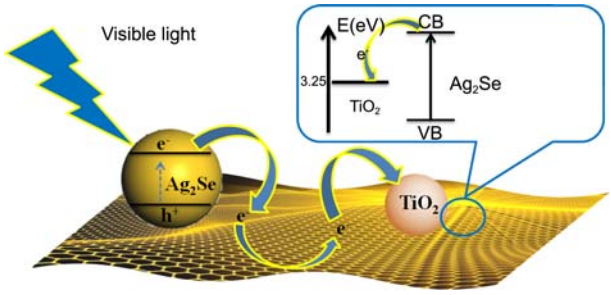


**Figure 9.** The scheme of excitation and charge transfer process between $TiO_2$ particles, $Ag_2Se$ particles and graphene nanosheet.

rated holes will be left in VB of $Ag_2Se$. In addition, graphene nanosheet acting as good electron acceptors[34,35] can accept the electrons by light irradiation and the electrons exited in CB of $Ag_2Se$ are also transferred to the surface of graphene. Thus the lifetime of the excited electrons ($e^-$) and holes ($h^+$) is prolonged in the transfer process, inducing higher quantum efficiency. The electrons can react with $O_2$ to generate $O_2^{\bullet-}$, and the holes theoretically migrate to the surface and react with $OH^-$ or $H_2O$ to generate $OH^{\bullet}$, these radicals can react with adsorbed pollutants. The reactions can be expressed as follows:

$$Ag_2Se\text{-}TiO_2 + h\nu \rightarrow Ag_2Se\ (e^-, h^+)\text{-}TiO_2 \quad (6)$$

$$Ag_2Se\ (e^-, h^+)\text{-}TiO_2 \rightarrow Ag_2Se\ (h^+)\text{-}TiO_2\ (e^-) \quad (7)$$

$$e^- + O_2 \rightarrow O_2^{\bullet-} \quad (8)$$

$$h^+ + H_2O \rightarrow OH^{\bullet} \quad (9)$$

$$h^+ + H_2O \rightarrow OH^{\bullet} + H^+ \quad (10)$$

$$O_2^{\bullet-} \text{ or } OH^{\bullet} + MB \rightarrow CO_2, H_2O \quad (11)$$

## Conclusions

In this study, we present the synthesis and characterization of $Ag_2Se$-Graphene/$TiO_2$ composites through a facile sonochemical method. The results showed that the $Ag_2Se$-Graphene/$TiO_2$ composites are able to exhibit high surface area, excellent structure, and great electrical and optical properties. The $Ag_2Se$-Graphene/$TiO_2$ composites showed an intense absorption and have a red-shifted absorption onset compared to pure $TiO_2$ and $Ag_2Se$-$TiO_2$. The excellent visible light photocatalytic activities of $Ag_2Se$-Graphene/$TiO_2$ for the degradation of Rh.B were higher than that of pure $TiO_2$. The high activity can be attributed to the synergetic effects of high charge mobility, and red shift in absorption edge of $Ag_2Se$-Graphene/$TiO_2$ composites.

## References

1. Geim, A. K.; Novoselov, K. S. *Nat. Mater.* **2007**, *6*, 183.
2. Kamat, P. V. *J. Phys. Chem. Lett.* **2010**, *1*, 520.
3. Zhang, H.; Lv, X.; Li, Y.; Wang, Y.; Li, J. *ACS Nano* **2010**, *4*, 380.
4. Kim,S. R.; Parvez, M. K.; Chhowalla, *M. Chem. Phys. Lett.* **2009**, *483*, 124.
5. Saleh, T. A.; Gondal, M. A.; Drmosh, Q. A. *Nanotechnology* **2010**, *21*, 495705.
6. Wang, S.; Shi, X. L.; Shao, G. Q.; Duan, X. L.; Yang, H.; Wang, T. G. *J. Phys. Chem. Solids* **2008**, *69*, 396.
7. Oh, W. C.; Jung, A. R.; Ko, W. B. *Mater. Sci. Eng. C* **2009**, *29*, 1338.
8. Oh, W. C., Zhang, F. J.; Chen, M. L. *J. Ing. Eng. Chem.* **2010**, *16*, 299.
9. Zhu, L.; Meng, Z. D.; Oh, W. C. *Chin. J. Catal.* **2011**, *32*, 926.
10. Woan, K.; Pyrgiotakis, G.; Sigmund, W. *Adv. Mater.* **2009**, *21*, 2233.
11. Chen, C.; Cai, W. M.; Long, M. C.; Zhou, B. X.; Wu, Y. H.; Wu, D. Y.; Feng, Y. J. *ACS Nano* **2010**, *4*, 6425
12. Zhang, H.; Lv, X. J.; Li, Y. M.; Wang, Y.; Li, J. H. *ACS Nano* **2010**, *4*, *380*.
13. Zhang, Y. H.; Tang, Z. R.; Fu, X. Z.; Xu, Y. J. *ACS Nano* **2010**, *4*, 7303.
14. Liang, Y. Y.; Wang, H. L.; Casalongue, H. N. S. C.; Chen, Z.; Dai, H. J. *Non Res.* **2010**, *3*, 701.
15. Hummers, W. S.; Offeman, R. E. *J. Am. Chem. Soc.* **1958**, *80*, 1339.
16. Marcano, D. C.; Kosynkin, D. V.; Berlin, J. M.; Sinitskii, A.; Sun, Z. Z.; Slesarev, A.; Alemany, L. B.; Lu, W.; Tour, J. M. *ACS Nano* **2010**, *4*, 4806.
17. Akhavan, O.; Abdolahad, M.; Esfandiar, A.; Mohatashamifar, M. *J. Phys. Chem. C* **2010**, *114*, 12955.
18. Vogel, R.; Pohl, K.; Weller, H. *Chem. Phys. Lett.* **1990**, *174*, 241.
19. Suleymanov, A. S. *Int. J. Hydrogen Energy* **1991**, *16*, 741.
20. Ennaoui, A.; Fiechter, S.; Tributsch, H.; Giersig, M.; Vogel, R.; Weller, H. *J. Electrochem. Soc.* **1992**, *139*, 2514.
21. Sheldrich, W. S.; Wachold, M. *Int. Ed. Engl.* **1997**, *36*, 206.
22. Das, V. D.; Karunakaran, D. *Phys. Rev. B* **1989**, *39*, 10872.
23. Zhao, J. J.; Jiang, B. T.; Zhang, S. Y.; Niu, H. L.; Jin, B. K.; Tian, Y. P. *Sci. China, Ser. B* **2009**, *52*, 2213.
24. Cao, H. Q.; Xiao, Y. J.; Lu, Y. X.; Yin, J. F.; Li, B. J.; Wu, S. S.; Wu, X. M. *Nano Res.* **2010**, *3*, 863.
25. Neppolian, B.; Bruno, A.; Bianchi, C. L.; Ashokkumar, M. *Ultrason Sonochem.* **2012**, *19*, 9.
26. Oh, W. C.; Chen, M. L.; Zhang, K.; Zhang, F. J.; Jang, W. K. *J. Korean Phys. Soc.* **2010**, *56*, 1097.
27. Zhan, J. H.; Yang, X. G.; Li, S. D.; Wang, D. W.; Xie, Y.; Qian, Y. T. *Int. J. Mater.* **2001**, *3*, 47.
28. Zhang, X. Y.; Li, H. P.; Cui, X. L.; Lin, Y. H. *J. Mater. Chem.* **2010**, *20*, 2801.
29. Zhang, H.; Lv, X. J.; Li, Y. M.; Wang, Y.; Li, J. H. *ACS Nano* **2010**, *4*, 380.
30. Bourlinos, A. B.; Gournis, D.; Petridis, D.; Szabo, T.; Szeri, A.; Dekany, I. *Langmuir* **2003**, *19*, 6050.
31. Qourzal, S.; Barka, N.; Tamimi, M.; Assabbane, A.; Nounah, A.; Ihlal, A.; Ait-Ichou, Y. *Mater. Sci. Eng. C* **2009**, *29*, 1616.
32. Yang, N. L.; Zhai, J.; Wang, D.; Chen, Y. S.; Jiang, L. *ACS Nano* **2010**, *4*, 887.
33. Li, Y.; Li, X.; Li, J.; Yin, J. *Water Res.* **2006**, *40*, 1119.
34. Williams, G.; Seger, B.; Kamat, P. V. *ACS Nano* **2008**, *2*, 1487.
35. Lightcap, I. V.; Kosel, T. H.; Kamat, P. V. *Nano Lett.* **2010**, *10*, 577.